Rapid oscillation and Fermi-surface reconstruction due to spin-density-wave formation in the organic conductor $(TMTSF)_2PF_6$

S. Uji
Tsukuba Magnet Laboratory, National Research Institute for Metals, Tsukuba, Ibaraki 305, Japan
and National High Magnetic Field Laboratory, Florida State University, Tallahassee, Florida 32306

J. S. Brooks and M. Chaparala
National High Magnetic Field Laboratory, Florida State University, Tallahassee, Florida 32306

S. Takasaki, J. Yamada, and H. Anzai
Himeji Institute of Technology, Akohgun, Hyogo 678-12, Japan
(Received 21 October 1996; revised manuscript received 27 January 1997)

Resistance and magnetic torque for the quasi-one-dimensional organic conductor $(TMTSF)_2PF_6$ have been measured over a wide magnetic field and temperature ranges to investigate the correlation between the rapid oscillation (RO) and the spin-density-wave (SDW) formation. The RO with the frequency of 220 T is found in the resistance above 15 T for all the current directions and in the *ab*-plane Hall resistance in the SDW phase. The RO amplitude has a sharp peak around 3 K, which is associated with a maximum of the normalized magnetoresistance. The magnetic torque shows a jump at the SDW transition temperature ($\sim$11.5 K) with decreasing temperature, and then a broad maximum around 3 K (T_{max}) suggesting a subphase transition. T_{max} slightly shifts to a high temperature with increasing magnetic field. A possible mechanism of the RO is discussed on the basis of the Fermi surface reconstruction due to the SDW formation. [S0163-1829(97)05018-2]

I. INTRODUCTION

The quasi-one-dimensional organic conductors $(TMTSF)_2X$, where TMTSF denotes tetramethyltetraselenafulvalene and $X=ClO_4$, PF_6, AsF_6, ReO_4, etc., have been of great interest because of many fascinating properties, such as superconductivity, quantum Hall effect, rapid oscillation (RO), and field-induced spin-density wave (FISDW) transitions.[1] The stacked platelike TMTSF molecules yield a highly anisotropic Fermi surface with only open sheets. For $X=PF_6$ and AsF_6, the ground state is the SDW phase at ambient pressure, but the SDW is suppressed and the superconducting state is induced by pressure. The SDW state is caused by the nesting of the two sheets of the one-dimensional (1D) Fermi surface [Fig. 1(a)]. The nesting vector **Q** for the PF_6 salt is determined to be incommensurate, $\mathbf{Q}(0.5, 0.24\pm0.3, -0.06\pm0.2)$ by NMR experiments.[2]

In the SDW phase, the possibility of subphase transitions has been reported. The spin-lattice relaxation rate $1/T_1$ of the proton in the TMTSF molecule for the PF_6 salt is found to show sharp drops at 3.7 K (T_{p1}) and 1.8 K (T_{p2}) when the magnetic field is larger than the spin-flop field ($\sim$0.5 T).[3] Below the spin-flop field, a sharp peak in $1/T_1$ is observed around 3 K.[4,5] These results suggest the presence of subphase transitions due to some change in the spin dynamics.[3] These transitions have been discussed in terms of some nesting vector change. Recently, $1/T_1$of Se NMR is also reported to show a sharp decrease below 4 K.[6] Another explanation of the proton $1/T_1$ anomalies around 3 K has been given by Clark *et al.*[7] They measured the temperature dependence of the proton $1/T_1$ carefully and claim that the 3.5 K anomaly is due to a dynamic effect rather than a phase transition. The dielectric constant shows a strong frequency dependence in the SDW phase for the PF_6 salt,[8,9] and it is ascribed to a critical slowing down towards a static glass transition near 2 K.[8] Long-time decay of the specific heat below 1 K indicates the possibility of low-energy excitation of the disordered SDW state,[10] which seems consistent with the glass-transition picture. At a high frequency (16.5 GHz), striking changes in the dielectric constant and conductivity are seen for the PF_6 and AsF_6 salts near 4 K.[11,12] These features are discussed in the framework of quasiparticle and condensate pictures. Nonlinear electric conductivity experiments for the AsF_6 salt shows a drastic increase of the threshold electric field around 3 K,[13] which strongly suggests some change of the pinning mechanism. On the other hand, the RO, which is periodic as a function of the inverse field, is seen in the magnetoresistance in the SDW phase and disappears at low temperatures.[14] This anomalous temperature dependence of the RO is expected to be correlated with the proposed subphase transitions. A similar behavior of the RO is also observed for the AsF_6 salt.[15,16]

The RO for the PF_6 and AsF_6 salts is detected only in the SDW phase. In contrast to these salts, the RO for the ClO_4 salt is observed in both the SDW and metallic (*M*) phases. The ClO_4 salt undergoes the ClO_4 anion order at 24 K with the superlattice (0,0.5,0) because of its lower symmetry. The superlattice potential separates the original Fermi surface into two zones and two pairs of open sheets of Fermi surface are consequently formed. The magnetic field along the c^* axis leads to the cascadelike FISDW transition. The final FISDW transition occurs at about 8 T. According to a new

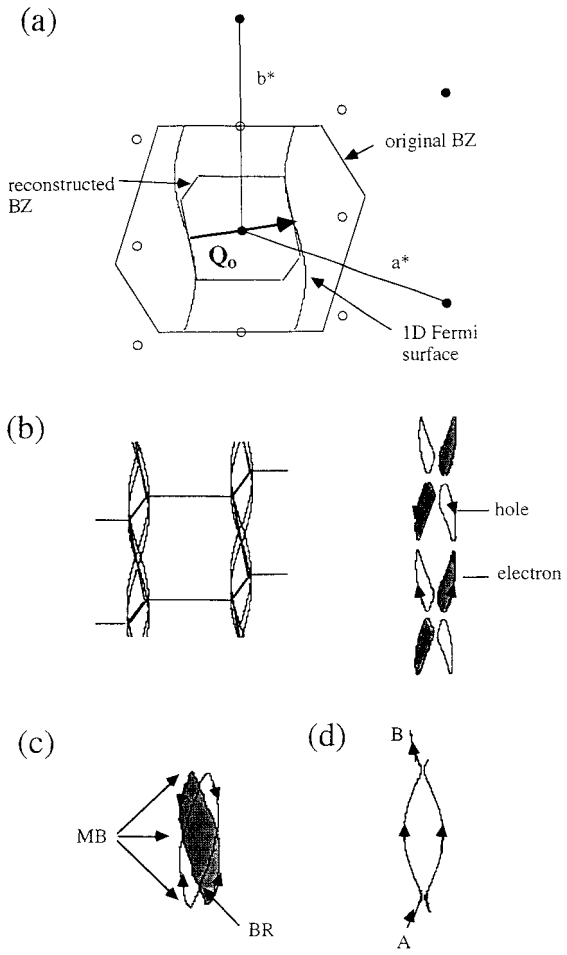

FIG. 1. (a) Schematic Fermi surface based on the original band-structure calculation for $(TMTSF)_2PF_6$. The warping of the 1D Fermi surface along the b^* direction is exaggerated. The thick arrow shows the commensurate nesting vector $\mathbf{Q}_0(1/2,1/4,0)$. The reconstructed Brillouin zone (BZ) boundary is also shown. The closed and open small circles indicate the reciprocal-lattice points in the original and reconstructed BZ's, respectively. (b) Reconstructed Fermi surface by the nesting. Electron and hole pockets formed by the imperfect nesting are shown. (c) Possible electron and hole orbits by the magnetic breakdown (MB) and Bragg reflection (BR) processes. (d) Two possible alternative trajectories causing quantum interference.

phase diagram,[17] the FISDW phase survives up to 31 T and a new phase boundary in the final FISDW phase is present. In the M phase, the RO is well understood in terms of quantum interference (QI) effect.[18] Two open sheets of the Fermi surface formed due to the anion order are very close to each other. Therefore, the magnetic breakdown (MB) easily takes place between the two sheets where the electrons travel along the same direction. This is the main reason why the QI is possible in the M phase. This interference is not expected for the PF_6 salt, because of no anion order. The origin of the RO in the main FISDW region between 8 and 28 T for the ClO_4 salt is still unclear. In the highest-field FISDW phase above 28 T, the reconstructed Fermi surface, based on the calculated band structure, gives the possibility of conventional SdH or dHvA effects coming from the MB closed orbits.[19] The temperature and field dependence of the RO is explained by Lifshitz-Kosevich (LK) formula with reasonable parameters. In the highest-field FISDW phase, the Fermi-surface sheets are expected to be almost perfectly nested with each other. In this sense, the electronic state in the SDW phase for the PF_6 salt may be similar to that in the highest-field FISDW phase for the ClO_4 salt.

Extensive studies have been made to understand the mechanism of the RO for the TMTSF system so far. However, the mechanism of the RO in the SDW phase is still an open question. In order to investigate the mechanism of the RO, and the relation between the SDW phase and the RO, we have made magnetoresistance and magnetization experiments over wide magnetic field and temperature ranges for the PF_6 salt.

II. EXPERIMENT

The single crystals of the PF_6 salt were synthesized electrochemically. The typical dimension of the single crystals is $\sim 3.0\times0.5\times0.5$ mm^3. The magnetic torque was measured by a torque magnetometer developed by Chaparala *et al.*[20] The magnetic field is tilted from the c^* axis (perpendicular to the conduction plane) of the sample by about 10° to detect large torque. The resistance was measured with electric current along all the crystal axes (a, b, and c) by a low-frequency ac technique. The magnetic field is applied along the c^* for the resistance measurements. Thin gold wires ($\phi 10$ μm) were attached to the sample using a silver paint. The same sample is used for the resistance measurements with the current parallel to the a and c axes ($I\|a$ and $I\|c$), and for the ab-plane Hall resistance measurements. All the resistance measurements were performed within a current region where the I-V property is linear. Different samples from the same batch were used for the b-axis resistance and the magnetic torque measurements. The sample temperature was controlled in ^{3}He and ^{4}He cryostats and measured by the vapor pressure and a calibrated Cernox sensor.

III. EXPERIMENTAL RESULTS

A. Resistance and RO

Figure 2 shows the temperature dependence of the resistivity for $I\|a$, b, and c axes. The contact configuration is also shown. The larger resistivity than the reported values is probably due to mechanical kinks. For all the current directions, the resistance shows a steep increase just below T_c, which is due to the decrease of the carriers by the Fermi-surface nesting. The resistance increases exponentially with an activation energy of about 16 K in the range between 2 and 8 K, but it saturates below $\sim$1.5 K. The overall behavior is consistent with previous reports.[3,9,21]

Figure 3 shows the magnetic-field dependences of the a-axis resistance at various temperatures. The magnetic field is applied parallel to the c^* axis (perpendicular to the ab plane). The magnetoresistance is positive in the whole temperature range. The RO is seen at high magnetic fields in the temperature range between 1.4 and 10 K. We note that the magnetoresistance seems the largest around 3 K. This behavior is closely correlated with the temperature dependence of the RO, as shown later. To see the RO more clearly, we plotted the derivative curves of the resistance $dR/d(1/B)$ (inset of Fig. 4). The RO is periodic as a function of the

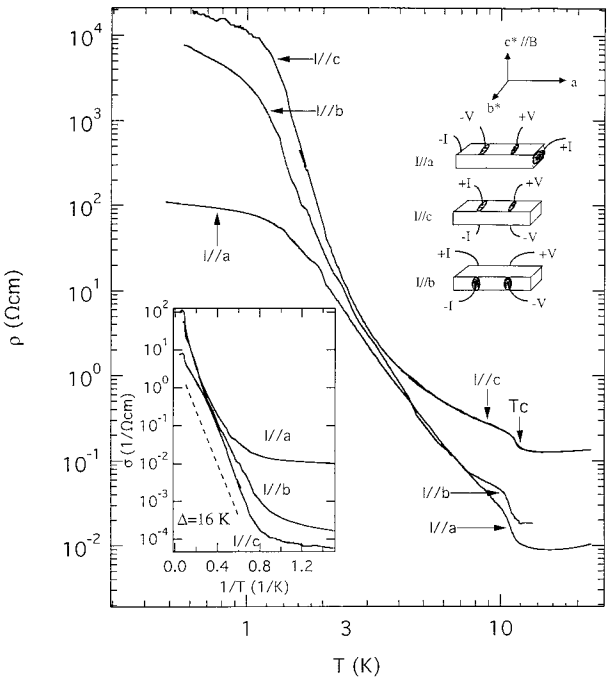

FIG. 2. Temperature dependence of the resistivity for $I\|a,b,c$ axes and contact configuration corresponding to each measurement. Inset: Conductivity vs $1/T$. The dotted line shows the thermal activation behavior with $\Delta=16$ K.

inverse field. The Fourier transform (FT) spectra of the RO between 15 and 30 T are shown in Fig. 4. The FT analysis shows that the second harmonic is slightly included in addition to the fundamental oscillation with the frequency of 220 T. The frequency agrees with the result reported by Ulmet *et al.*[14] The frequency is temperature independent.

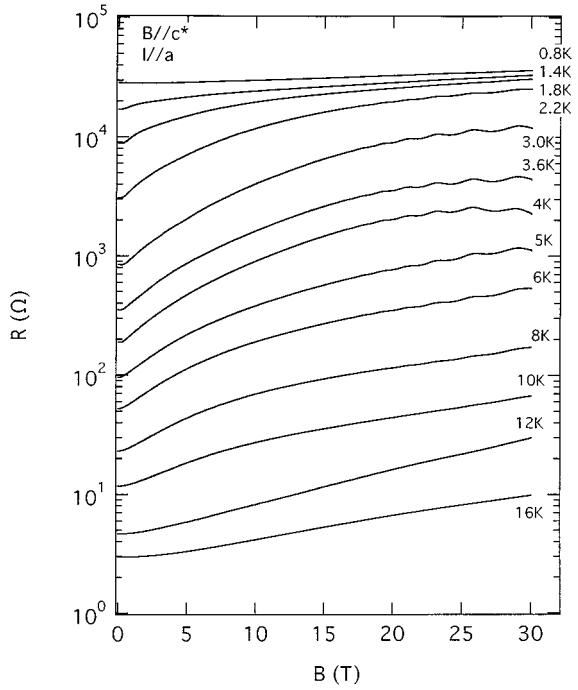

FIG. 3. Magnetic-field dependence of the resistance for $I\|a$ at various temperatures. The magnetic field is applied parallel to the c^* axis.

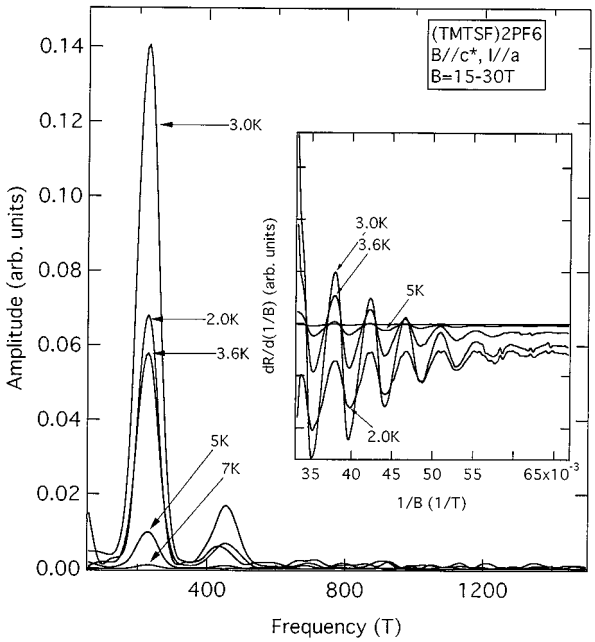

FIG. 4. FT spectra of the derivative curve of the a-axis resistance in the magnetic-field range between 15 and 30 T. The fundamental frequency is 220 T. Inset: Derivative curves of the resistance.

The RO can be observed for all the current directions. For comparison, the data at 3 K are shown in Fig. 5. $R(B)/R(0)$ is the smallest for $I\|c$ and the largest (up to $\sim$300) for $I\|b$. The magnetoresistance keeps increasing up to 30 T for all the current directions. This point will be discussed later. The RO normalized by the nonoscillatory background R_0 is plotted in the inset. The RO amplitude rises up

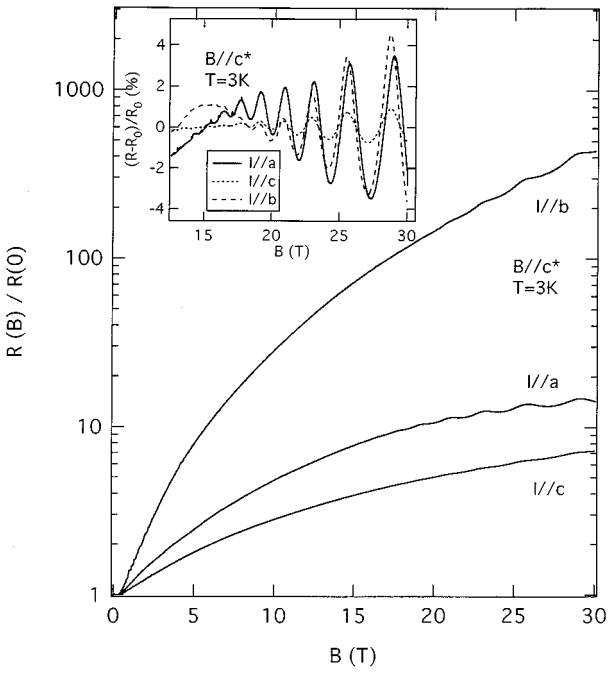

FIG. 5. Normalized resistance at 3 K for $I\|a,b,c$ axes. The field is parallel to the c^* axis. Inset: Oscillatory part of the resistance normalized by the nonoscillatory background R_0.

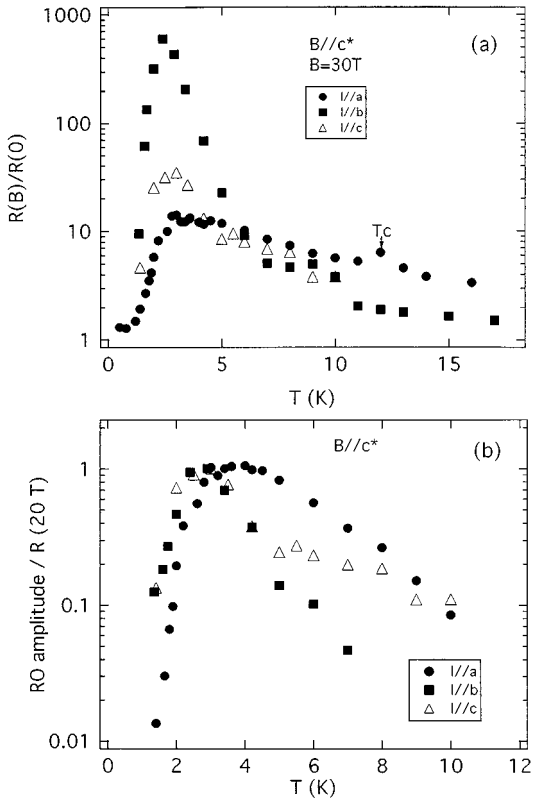

FIG. 6. (a) Temperature dependence of the normalized magnetoresistance $R(B)/R(0)$ at 30 T. (b) Temperature dependence of the RO amplitude with the fundamental frequency. The amplitude is obtained from the FT in the field range 15–30 T (inset of Fig. 4). The amplitude is divided by the background resistance at 20 T and then normalized by the maximum value.

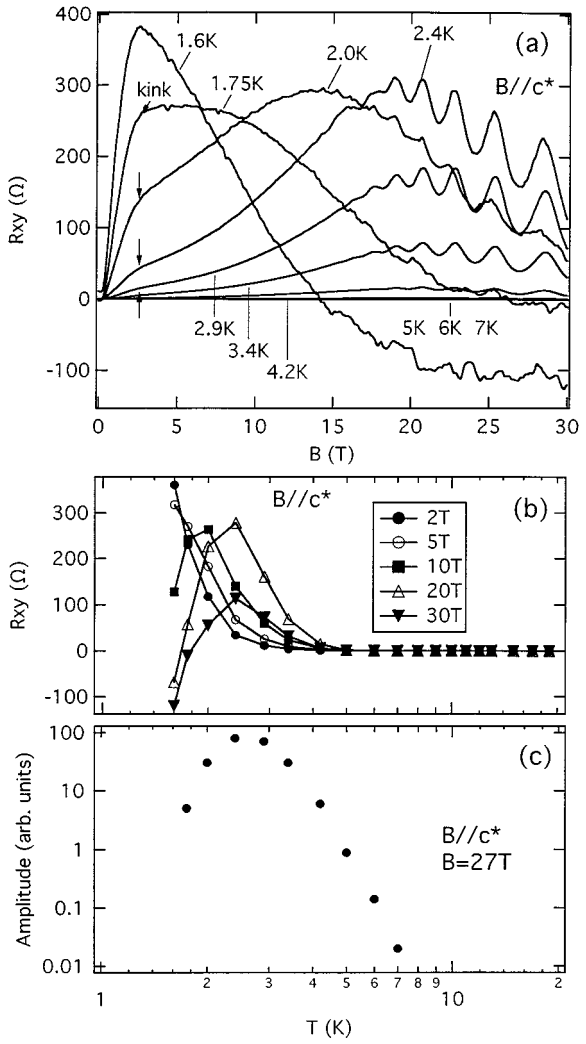

FIG. 7. (a) Hall resistance in the ab plane at various temperatures. Arrows indicate the kink position in the Hall resistance. (b) Temperature dependence of the Hall resistance. (c) Temperature dependence of the RO amplitude at 27 T.

to 4% around 28 T for $I\|a$ and $I\|b$, but is only 1% for $I\|c$ (note that the same sample is used for the $I\|a$ and $I\|c$ experiments). The slight frequency difference is probably due to a sample alignment.

Figure 6(a) shows the temperature dependence of the normalized magnetoresistance $R(B)/R(0)$ for $I\|a,b,c$ axes at 30 T. As the temperature decreases, $R(B)/R(0)$ gradually increases, has a maximum around 3 K, and then steeply drops below 2.5 K. The temperature dependence of the RO amplitude with the fundamental frequency (220 T) divided by the background resistance at 20 T, which is the center field of the FT region, is presented in Fig. 6(b). The oscillation amplitudes have maxima at the same temperature, ~3.5 K, and quickly go down below it. The second harmonic shows similar behavior. The fact that the RO amplitude has a maximum was first observed by Ulmet *et al.*[14] They reported that the RO vanishes very quickly between 4.2 and 5 K, and pointed out the possibility of a phase transition. In our case, the temperature of the amplitude maximum is lower than their result. Recently, the maxima of the normalized magnetoresistance and the RO amplitude for $I\|a$ are also reported for the AsF_6 salt.[15,16]

A similar sharp maximum of the RO amplitude has been observed in the SDW phase for the relaxed ClO_4 salt.[19] For the ClO_4 salt, the RO has a steep decrease below 2 K. A large hysteresis due to the FISDW transition is observed in the magnetoresistance below 2 K and the normalized magnetoresistance does not change very much below 2 K.[18] However, for the PF_6 salt, no hysteresis is found and the temperature dependence of the RO is clearly correlated with that of the magnetoresistance.

B. Hall resistance

Figure 7(a) shows the Hall resistance in the ab plane at various temperatures. The absolute value of the Hall resistance below 2 K is somewhat ambiguous because of the high ab-plane resistance. At 1.6 K, the Hall resistance quickly goes up with increasing field, has a peak at ~2.5 T and then decreases. As temperature increases, the peak becomes broad, and the field where the Hall resistance has a peak shifts to a high field. A kink behavior is seen around 2.5 T above 1.75 K and remains there up to 3.4 K as shown by arrows. The RO can be observed above ~15 T at temperatures between 1.8 and 7 K. At 1.6 K, the RO is less than the noise level.

The temperature dependence of the Hall resistance is shown in Fig. 7(b). The Hall resistance monotonically in-

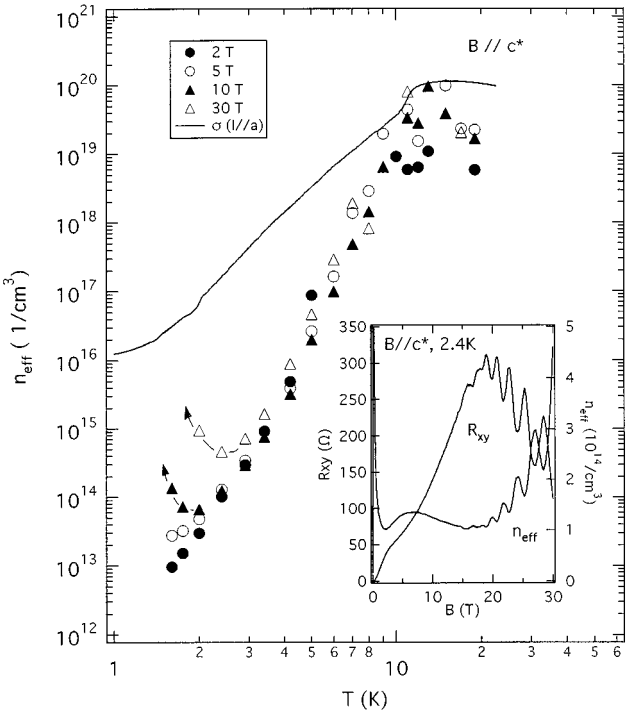

FIG. 8. Temperature dependence of the effective carrier concentration n_{eff} derived from the Hall resistance at several fields. The conductivity along the a axis is shown by a solid line for comparison. Inset: Field dependence of the ab-plane Hall resistance and n_{eff} at 2.4 K.

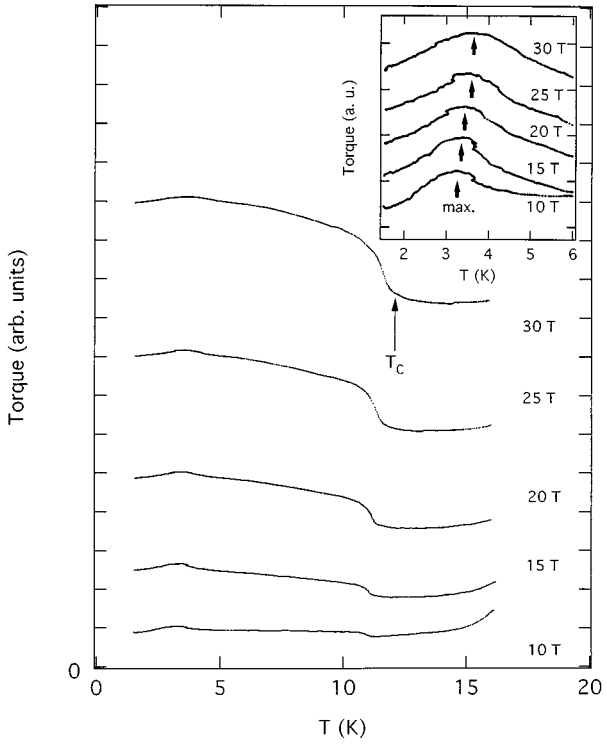

FIG. 9. Magnetic torque measured by a cantilever technique. The magnetic field is tilted from the c^* axis by about 10°. The arrow shows the SDW transition. The inset presents the expanded picture around 3 K, where the maxima are evident. The data in the inset are shifted.

creases with decreasing temperature below 5 T, but has a maximum around 2 K above 5 T. The RO amplitude in the Hall resistance has a sharp peak at 2.5 K [Fig. 7(c)], which is similar to those in the a-, b- and c-axis resistance. The second harmonic is not evident in the Hall resistance.

From the relation $R_{\mathrm{Hall}}=1/n_{\mathrm{eff}}ec$ in the high-field limit, where R_{Hall} is the Hall resistivity, we can estimate the effective carrier concentration n_{eff}. n_{eff} is given by n_p-n_e, where n_p and n_e are the hole and electron carrier concentrations, respectively. Figure 8 presents the temperature dependence of n_{eff} at several fields. For comparison, the conductivity for $I\|a$ is also shown in arbitrary units. The field dependence of the Hall resistance and calculated n_{eff} at 2.4 K is shown in the inset of Fig. 8. Below T_c, n_{eff} steeply decreases with decreasing temperature. This behavior qualitatively agrees with the temperature dependence of the conductivity. Judging from the stoichiometry (one carrier in one unit cell), the carrier concentration is estimated to be $1.4\times10^{21}/\mathrm{cm}^3$. The experimental value $\sim10^{20}/\mathrm{cm}^3$ at $\sim$15 K may be rather small as compared with the estimated value. We believe that this difference is within the experimental error because the contact configuration and the sample shape are not ideal. We note that n_{eff} is much smaller than that expected from the conductivity at lower temperatures.

C. Magnetic torque

Figure 9 shows the temperature dependence of the magnetic torque at various fields. We see a steep increase of the torque around 11.5 K (T_c), which is ascribed to the transition to the SDW phase. This transition shifts to a high temperature as the field increases, which is consistent with the results reported by a few groups.[22,23] This behavior is understood in terms of the stabilization of the SDW state by the magnetic field. In addition to this transition, a broad maximum is seen around 3 K. The data around 3 K are expanded in the inset. The maximum position T_{max} also shifts to a higher temperature with increasing field.

The magnetic torque measured by this technique is given by $B(M_{\|}^2-M_{\perp}^2)/M$ where $M_{\|}$ and $M_{\perp}$ are the components of the magnetization parallel and perpendicular to the c^* axis, respectively, and M the component along the field. The magnetization has been measured for the PF_6 (Ref. 24) and AsF_6 salts.[25] Above the spin-flop field, the magnetization is almost isotropic in the metallic phase but becomes more anisotropic in the SDW phase. The c-axis component of the static magnetization ($M_{\|}$) is larger than $M_{\perp}$. Therefore, $M_{\|}^2-M_{\perp}^2$ is expected to be positive and larger in the SDW phase than in the M phase. This is consistent with the torque results.

The change of the torque at T_c grows rapidly as the field increases. However, the peak height at 3 K does not seem sensitive to the applied field. No significant hysteresis has been found at 3 K and T_c, suggesting that both transitions are the second order in nature. We have tried the torque measurements for three different samples up to 30 T, but no RO has been found in the torque.

D. *T*-*B* phase diagram

The maximum in the magnetization around 3 K suggests the presence of a subphase transition in the main SDW

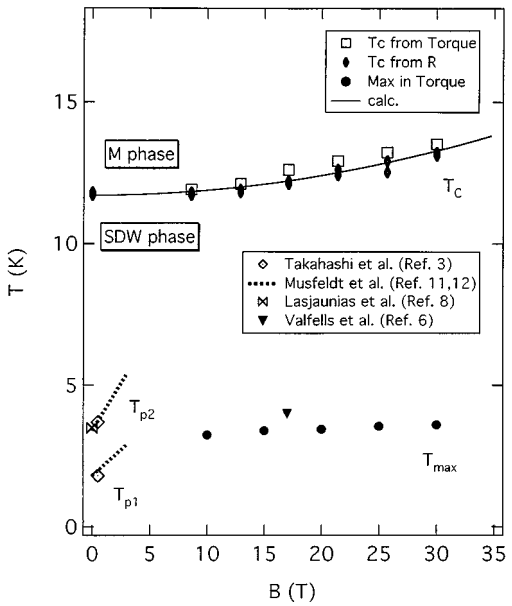

FIG. 10. Temperature-field phase diagram. $T_{\max}$, where the torque has a maximum, and T_c determined from the magnetic torque and resistance measurements are shown. The solid line shows the B^2 dependence. Temperatures (T_{p1} and T_{p2}), where several experiments show anomalies, are also shown.

phase. In Fig. 10, $T_{\max}$, where the torque has a maximum, and T_c determined from the torque and resistance measurements are shown. T_c quadratically increases with increasing field, which is consistent with the reported results.[22,23] The temperatures (T_{p1} and T_{p2}) where some experiments show anomalies are also shown. According to the dielectric constant experiments,[11,12] both the temperatures increase with increasing field as shown by dotted lines. At present, it is not obvious whether $T_{\max}$ corresponds to T_{p1} or T_{p2}.

IV. DISCUSSION

A. Possible mechanism of RO

The RO is observed in the resistance for all the current directions and in the ab-plane Hall resistance. The RO amplitude steeply decreases below $\sim$3 K, which is probably related to a subphase transition as suggested from several experiments. In this section, we discuss the reconstruction of the Fermi surface due to the SDW formation and a possible mechanism of the RO.

The NMR and μSR experiments show that the SDW periodicity is incommensurate[2,26,27] although very close to the commensurate one, $\mathbf{Q}_0(1/2,1/4,0)$.[2] Provided with the commensurate nesting vector $\mathbf{Q}_0$, we can reconstruct the Fermi surface in the SDW phase as shown in Fig. 1(b). The original Fermi surface is based on the band calculation,[28] but the warping along the b axis is exaggerated. In the reconstructed Fermi surface, the two different small pockets, electron and hole pockets are formed as long as the nesting is not perfect. The reconstructed Fermi surface is accidentally very similar to that for the ClO_4 salt, in which the nesting vector (1/2,0,0) is assumed.[19]

The resistivity exponentially increases with decreasing temperature below T_c and has very large values at low temperatures. This fact shows that the pockets formed by the imperfect nesting should be very small. It is probably impossible to observe the low-frequency SdH oscillations corresponding to such very small pockets. As long as the nesting vector is close to $\mathbf{Q}_0$, the electron and hole pockets must have the same area, i.e., this system is compensated. On the other hand, if the magnetic field is high enough, magnetic breakdown (MB) takes place. In this case, as shown in Fig. 1(c), two large MB orbits (electron and hole orbits) are formed. If the sample quality is high enough, we should observe the SdH oscillations corresponding to those MB orbits in all the components of the resistivity tensor ($\rho_{xx}, \rho_{yy}, \rho_{xy}, \ldots$). The MB orbits may be as large as 3% of the original Brillouin zone, which corresponds to the RO frequency (220 T). Both the electron and hole MB orbits also have the same area, so that the system remains compensated. Therefore, the magnetoresistance should not saturate for all the current directions. Actually, the magnetoresistance does not saturate up to 30 T in the range between 3 K and T_c for all the current directions. The possibility of the MB is discussed later.

The carrier concentration n_{eff} derived from the Hall resistance decreases more quickly below T_c than the conductivity σ (Fig. 8). In the diagonal conductivity ($\sigma = ne^2\tau/m^*$), the number of carriers n is given by $n_h + n_e$ in contrast to $n_{\text{eff}} = n_h - n_e$ in the Hall conductivity. If the system is compensated, we can expect $n_{\text{eff}} \ll n$. This explains the fact that n_{eff} is much smaller than that expected from σ at low temperatures (Fig. 8).

If the observed RO is the conventional SdH oscillation, the effective mass is approximately derived from the temperature dependence of the RO amplitude on the assumption of a constant Dingle temperature, i.e., scattering time. Figure 11 shows so-called mass plots, i.e., the normalized amplitude divided by temperature is plotted against temperature. In this temperature range, the scattering time is not expected to depend on temperature strongly. The solid lines are the calculated results with the LK formula.[29] The effective mass obtained ranges from $0.8m_0$ to $1.3m_0$. The different effective masses for different current directions are unphysical because the SdH oscillations result from the same cyclotron motion. The mass plot for the SdH oscillation is strictly valid only when one current path is present in the system. In addition to the MB process, the thermally activated process in the conductivity, which is current direction dependent and causes a nonoscillatory temperature-dependent background, is present in parallel, so that it is difficult to obtain the contribution of the MB process only. This is a possible reason why the effective mass seems different for each current direction. For the ClO_4 salt, the temperature and field dependence of the RO has been analyzed in the SDW and M phases.[18,19] The behavior of the RO is well explained on the assumption of the effective mass of 1.0–$1.3m_0$. Therefore, the obtained mass for the PF_6 salt may be reasonable in spite of the oversimplified analysis.

The RO amplitude steeply decreases with decreasing temperature below $\sim$3 K. If this transition is caused by a slight change of the nesting vector as suggested from the NMR experiments, the area of the closed orbits changes because the formation of the closed orbits is very sensitive to the nesting vector. It should cause a significant phase smearing

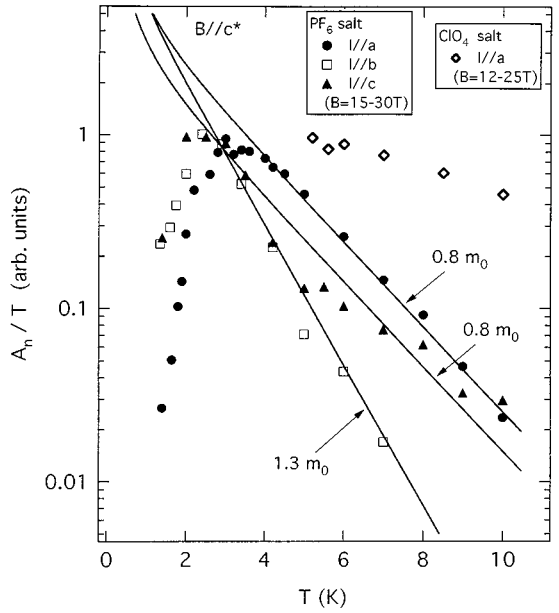

FIG. 11. Mass plots for $B\|c^*$. The RO amplitude normalized by $R(20\ \mathrm{T})$ and then divided by temperature is plotted against temperature. The solid lines are the calculated results with LK formula. The obtained effective mass ranges from $0.8m_0$ to $1.3m_0$. The normalized RO amplitude divided by temperature in the M phase for the ClO_4 salt is shown for comparison, which results from the QI effect (Ref. 18).

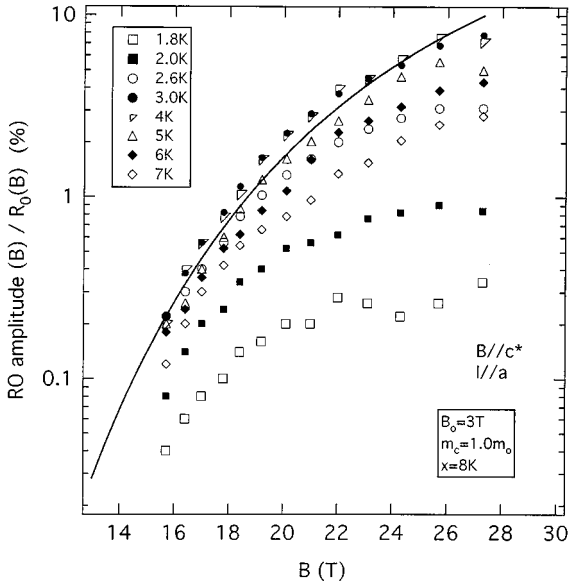

FIG. 12. Magnetic-field dependence of the RO amplitude for $I\|a$. The solid line is the fitted result with the LK formula on the basis of the MB and BR processes.

effect on the SdH oscillation. In addition, the carrier compensation is removed by the change of the nesting. The steep decrease of the RO amplitude and the normalized magnetoresistance below 3 K for all the directions seems consistent with this picture.

An alternative picture with respect to the 3.5 K anomalies is a glass transition.[8–10] The dielectric constant and heat-capacity experiments suggest some critical slowing down around 3 K. Within this model, the SDW is pinned on random impurities, and many grains, where the SDW phase is coherent, are present. The origin of such grains is not clear. If there exist many metastable configurations of the grains, the fluctuation from one metastable state to another may take place within a characteristic time scale. As the temperature decreases, the fluctuation will be frozen. If such grains exist, the grain size must be much larger than the cyclotron orbit, whose radius is about 200 A at 25 T, for the observation of the SdH oscillation because of scattering of the electrons at the grain boundaries. It is not clear whether the rapid decrease of the RO amplitude and the normalized magnetoresistance below 3 K is consistent with the glass-transition model.

Another possibility of the mechanism of the RO is the quantum interference (QI) effect.[29,30] As shown in Fig. 1(d), there are two alternative trajectories for the electron motion. When one electron travels from point A to point B, the QI occurs. In this case, however, the temperature dependence of the amplitude in this temperature range is expected to be much smaller than the experimental results. For comparison, the temperature dependence of the RO amplitude observed in the M phase for the ClO_4 salt is shown in Fig. 11. We have claimed that the RO in the M phase for the ClO_4 salt is caused by the QI effect and the temperature dependence of the RO amplitude results from that of the scattering time.[18] The large difference of the temperature dependence from the ClO_4 case suggests that the QI is not the main mechanism of the RO for the PF_6 salt.

B. Field dependence of RO

In the model shown in Fig. 1(c), the MB process is necessary for the observation of the RO. The MB probability[29] is given by

$$p=\exp(-B_0/B),$$

$$B_0\approx\frac{m_c c}{\hbar e}\frac{\Delta^2}{E_F\sin(2\theta)},$$

where B_0 is the MB field, Δ is the energy gap, and the E_F is the Fermi energy before the SDW formation. θ is the scattering angle at the gap. It is not easy to estimate θ precisely because it is very sensitive to the shape of the original Fermi surface. The term $\sin(2\theta)$ may range from 1 to 0.05. The NMR and μSR results shows that the order parameter, i.e., the energy gap Δ is almost constant below 10 K.[2,27] Assuming $\Delta=16$ K (Fig. 2), and $E_F=0.1$ eV, B_0 is estimated to be only 3 T even for $\sin(2\theta)=0.1$. This suggests that the MB easily takes place. The orbits shown in Fig. 1(c) include four MB and two Bragg reflection (BR) processes. The BR probability is $(1-p)$, so the total probability of the cyclotron motion along these electron and hole orbits is given by $p^4(1-p)^2$. In Fig. 12, the field dependence of the RO amplitude and the fitted result for the 4-K data (solid line) are shown. In this calculation, we used m_c(effective mass $=1.0m_0$, x (Dingle temperature)$=8$ K, and $B_0=3$ T. The agreement with the experimental result is satisfactory. However, the field dependence of the RO below 2 K cannot be reproduced well by this model with the same parameters, because the field dependence is much smaller than that above 2 K.

The reconstructed Fermi surface is very complicated, so that the field dependence of the resistance and Hall resistance

cannot be compared with the calculation for a standard model.[29] However, we can expect that the MB effectively increases n_{eff} with increasing field. The increase of n_{eff} at high fields ($B>20$ T) shown in the inset of Fig. 8 may be due to the MB effect.

The Fermi surface shown in Fig. 1(c) is reconstructed on the assumption of the commensurate nesting vector. When it is incommensurate, the reconstructed Fermi surface cannot be displayed, because of the mismatch between the lattice periodicity and the SDW modulation. However, as long as the SDW modulation is very close to the commensurate, similar MB orbits may be formed, i.e., the SdH oscillations corresponding to the MB orbits as shown in Fig. 1(c) may be observable.

V. CONCLUSION

We have reported the resistance and the magnetic torque results over wide field and temperature ranges for $(TMTSF)_2PF_6$. Assuming the commensurate nesting vector close to the incommensurate one determined by the NMR experiment, we reconstructed the Fermi surface based on the calculated band structure in the SDW phase. In the reconstructed Fermi surface, small electron and hole orbits are formed, whose areas are almost the same, i.e., the carrier of the system is almost compensated. At high fields, the MB takes place, so the carriers travel along the large MB closed orbits. The system still remains compensated. This model explains well the large magnetoresistance for all the current directions and the large Hall resistance in the temperature region where the RO is seen. We proposed that the RO is ascribed to the conventional SdH oscillation coming from the MB orbits in the reconstructed Fermi surface. The temperature and field dependence of the RO is consistent with this model. The steep decreases of the RO amplitude and the normalized magnetoresistance blow $\sim$3 K are understood in terms of some change of the nesting vector.

ACKNOWLEDGMENTS

We would like to thank P. M. Chaikin, M. Naughton, and J. Musfeldt for helpful discussions. The high magnetic field experiments were carried out at National High Magnetic Field Laboratory at Florida State University. This study was partially supported by NSF DMR 95-10427.

[1] For a review, see T. Ishiguro and K. Yamaji, *Organic Superconductors* (Springer-Verlag, Berlin, 1990).
[2] T. Takahashi, Y. Maniwa, H. Kawamura, and G. Saito, J. Phys. Soc. Jpn. **55**, 1364 (1986).
[3] T. Takahashi, T. Harada, Y. Kobayashi, K. Kanoda, K. Suzuki, K. Murata, and G. Saito, Synth. Met. **41-43**, 107 (1985).
[4] K. Hiruma, T. Nakamura, and T. Takahashi, Synth. Met. (to be published).
[5] K. Nomura, Y. Hosokawa, T. Sekiguchi, S. Takasaki, J. Yamada, S. Nakatsuji, and H. Anzai, Synth. Met. (to be published).
[6] S. Valfells, P. Kuhns, A. Kleinhammes, W. Moulton, J. S. Brooks, S. Takasaki, J. Yamada, H. Anzai, and S. Uji, Synth. Met. (to be published).
[7] W. G. Clark, M. E. Hanson, W. H. Wong, and B. Alavi, J. Phys. (France) IV **3**, 235 (1993).
[8] L. C. Lasjaunias, K. Biljakovic, P. Monceau, and K. Bechgaad, Phys. Rev. B **53**, 7699 (1996).
[9] F. Nad, P. Monceau, and K. Bechgaad, Solid State Commun. **95**, 655 (1995).
[10] L. C. Lasjaunias, K. Biljakovic, F. Nad, P. Monceau, and K. Bechgaad, Phys. Rev. **72**, 1283 (1994).
[11] J. L. Musfeldt, M. Poirier, P. Batail, and C. Lenoir, Phys. Rev. B **51**, 8347 (1995).
[12] J. L. Musfeldt, M. Poirier, P. Batail, and C. Lenoir, Phys. Rev. B **52**, 15 983 (1995).
[13] M. Nagasawa, T. Sambongi, K. Nomura, and H. Anzai, Solid State Commun. **93**, 33 (1995).
[14] J. P. Ulmet, L. Bachere, and S. Askenazy, Solid State Commun. **58**, 753 (1986); J. P. Ulmet, P. Auban, A. Khmou, S. Askenazy, and A. Moradpour, J. Phys. Lett. (Paris) **46**, 535 (1985).
[15] J. P. Ulmet, A. Narjis, M. J. Naughton, and J. M. Fabre, Phys. Rev. B **55**, 3024 (1997); J. P. Ulmet *et al.*, Synth. Met. (to be published).
[16] M. Naughton, J. P. Ulmet, I. J. Lee, and J. M. Fabre, Synth. Met. (to be published).
[17] S. K. Mckernan, S. T. Hannahs, U. M. Scheven, G. M. Danner, and P. M. Chaikin, Phys. Rev. Lett. **75**, 1630 (1995).
[18] S. Uji, T. Terashima, H. Aoki, J. S. Brooks, M. Tokumoto, S. Takasaki, J. Yamada, and H. Anzai, Phys. Rev. B **53**, 14 399 (1996).
[19] J. S. Brooks, R. G. Clark, R. H. Mckenzie, R. Newbury, R. P. Starret, A. V. Skougarevsky, M. Tokumoto, S. Takasaki, J. Yamada, H. Anzai, and S. Uji, Phys. Rev. B **53**, 14 406 (1996).
[20] M. Chaparala, O. H. Chung, M. J. Naughton, in *Superconductivity and Its Applications*, edited by H.-S. Kuck, D. T. Shaw, and M. J. Naughton, AIP Conf. Proc. No. 273 (AIP, New York, 1993), p. 407.
[21] K. Bechgaard, C. S. Jacobsen, K. Mortensen, J. H. Pederson, and N. Thorup, Solid State Commun. **33**, 1119 (1980).
[22] N. Biskup, S. Tomic, and D. Jerome, Phys. Rev. B **51**, 17 972 (1995).
[23] G. M. Danner, P. M. Chaikin, and S. T. Hannahs, Phys. Rev. B **53**, 2727 (1996).
[24] K. Mortensen, Y. Tomkiewicz, T. D. Schultz, and E. M. Engler, Phys. Rev. Lett. **46**, 1234 (1981).
[25] K. Mortensen, Y. Tomkiewicz, and K. Bechgaard, Phys. Rev. B **25**, 3319 (1982).
[26] E. Barthel, G. Quirion, P. Wzietek, D. Jerome, J. B. Christensen, M. Jorgensen, and K. Bechgaad, Europhys. Lett. **21**, 37 (1993).
[27] I. P. Le, A. Karen, G. M. Luke, B. J. Sternlieb, W. D. Wu, Y. J. Uemura, J. H. Brewer, T. M. Piseman, R. V. Upasani, L. Y. Chiang, W. Kang, P. M. Chaikin, T. Csiba, and G. Gruner, Phys. Rev. B **48**, 7284 (1993).
[28] P. M. Grant, J. Phys. (Paris) Colloq. **4**, C3-847 (1983).
[29] D. Shoenberg, *Magnetic Oscillations in Metals* (Cambridge University Press, Cambridge, England, 1984).
[30] R. W. Stark and C. B. Friedberg, J. Low Temp. Phys. **14**, 111 (1974).